Editors' Suggestion | Featured in Physics

Quantum Gas Microscopy of Fermions in the Continuum

Tim de Jongh,[1,*] Joris Verstraten,[1,*] Maxime Dixmerias,[1] Cyprien Daix,[1] Bruno Peaudecerf,[2] and Tarik Yefsah[1]
[1]Laboratoire Kastler Brossel, ENS-Université PSL, CNRS, Sorbonne Université, Collège de France, 24 rue Lhomond, 75005 Paris, France
[2]Laboratoire Collisions Agrégats Réactivité, UMR 5589, FERMI, UT3, Université de Toulouse, CNRS, 118 Route de Narbonne, 31062, Toulouse CEDEX 09, France

(Received 14 November 2024; revised 23 January 2025; accepted 20 February 2025; published 5 May 2025)

Atom-based quantum simulators offer a unique platform that enables the imaging of each particle in a many-body system. Until now, however, this capability has been limited to quantum systems in discretized space such as optical lattices and tweezers, where spatial degrees of freedom are quantized. Here, we introduce a novel method for imaging atomic quantum many-body systems in the continuum, allowing for *in situ* resolution of every particle. We demonstrate the capabilities of our approach on a two-dimensional atomic Fermi gas. We probe the density correlation functions, resolving their full spatial functional form, and reveal the shape of the Fermi hole arising from Pauli exclusion as a function of temperature. Our method opens the door to probing strongly correlated quantum gases in the continuum with unprecedented spatial resolution, providing *in situ* access to spatially resolved correlation functions of arbitrarily high order across the entire system.

DOI: 10.1103/PhysRevLett.134.183403

Atom-based quantum simulators provide a unique approach to obtaining quantitative knowledge on the microscopic properties of correlated quantum systems, with a high level of control and ever improving imaging capabilities, which in many cases allow resolving each constituent of the system [1–4]. For instance, ultracold atoms and molecules in optical lattices allow for the exploration of Hubbard models, critically important in the context of high-T_c superconductivity [1,2,5–10]. Tweezer-trapped few-particle systems have enabled studying the buildup of complexity and many-body effects in mesoscopic fermionic clusters, directly relevant to the physics of atomic nuclei [11–15]. Tweezer arrays of Rydberg atoms and dipolar molecules offer the ability to explore many-body states with long-range interactions and pristine internal state control, allowing for the investigation of a wide class of spin models [3,16–20]. All of these platforms feature single-particle (atom or molecule) imaging giving direct access to the microscopic properties of the system.

Another important class of quantum gas experiments addresses quantum matter in the bulk, that is, with large ensemble of particles in homogeneous or weakly varying traps, and have had great success in studying several key paradigms of many-body and statistical physics. Prominent examples include studies of fermionic superfluidity in the BEC-BCS crossover [21–25], Berezinksii-Kosterlitz-Thouless topological order [26–30], Kibble-Zurek critical dynamics near second-order phase transitions [31–33], and supersolid behaviors in Bose gases [34–38]. Recently, the creation of Bose-Einstein condensates of dipolar molecules opened a whole new window of exploration for exotic phases of quantum matter [39]. So far, however, the imaging techniques available in these experiments only gave access to average density distributions, and have largely limited their scope to the exploration of global coherence, thermodynamic, or transport properties [24,25,32,38].

Here, we introduce quantum gas microscopy in the continuum. We apply it to a two-dimensional (2D) Fermi gas where we spatially resolve each atom in the system *in situ* (see Fig. 1). We measure the full functional form of the two- and three-point spatial density correlation functions, revealing the shape of the Fermi hole due to the Pauli exclusion principle as well as its temperature dependence. We study the system in the noninteracting regime, which allows us to directly compare the measured correlation functions to theoretical predictions, finding excellent agreement. Furthermore, without relying on any fitting, we directly cross-validate the measurements of the two- and three-point correlation functions by relating them through Wick's theorem [40], which is expected to hold for our samples, obtaining excellent agreement and thus a stringent validation of our imaging method. Finally, we depart from the pure 2D case by allowing fermions to populate quantum states in the third direction of motion and show that correlation functions offer a pristine way to characterize populations in these transverse motional levels. These measurements represent the first *in situ* and atom-resolved spatial correlation measurements of a bulk gas. The general

*These authors contributed equally to this work.

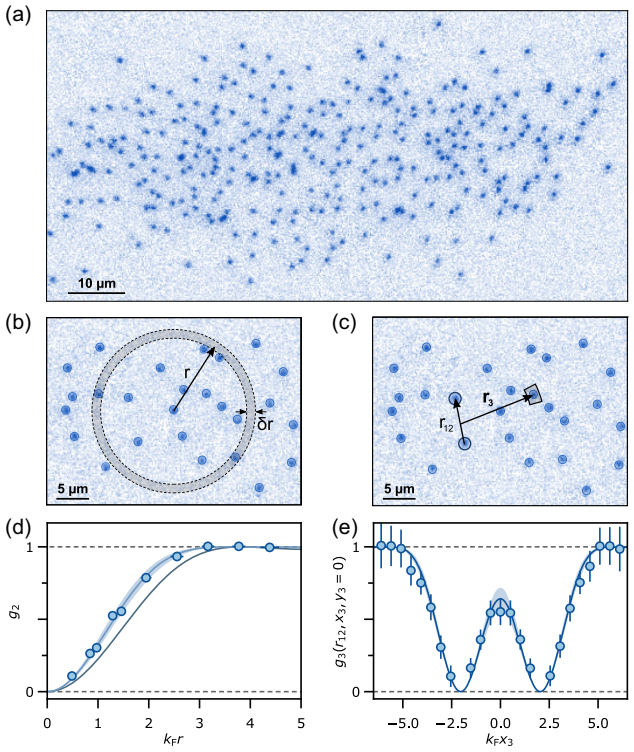

FIG. 1. Probing *in situ* correlations in the continuum. (a) Single-atom image of a noninteracting Fermi gas of $N = 331$ atoms. (b) Extraction of the g_2 correlation function from the experimental images. Identified atoms are marked by blue circles. For each atom, we count the number of surrounding atoms at a distance between r and $r + \delta r$, as indicated by the dashed circles. (c) Extraction of the g_3 correlation function. We identify all pairs with certain distance r_{12}. For each of these pairs, we register the position $\mathbf{r}_3 = (x_3, y_3)$ of each surrounding atom, relative to the center of mass of the pair. (d) Example of measured density-density correlation function $g_2(r)$ (blue circles), zero-temperature prediction (gray line), and theoretical fit yielding $T/T_F = 0.47(4)$ (blue line, shaded area indicating uncertainty [41]). (e) Experimental g_3 for $r_{12} = 4.1k_F^{-1}$ with the third atom positioned along the interparticle axis of the pair ($\mathbf{r}_{12}$), and theory at $T/T_F = 0.47$ (solid line and shaded area). Error bars show the standard error of the mean [41].

approach introduced here is readily applicable to probe strongly interacting quantum gases.

Challenges—Quantum gas microscopy was initially developed in the context of Hubbard physics [5,6] and has so far been devoted to the study of lattice and spin-chain systems [1,2], where atoms initially evolve in a discretized space and can tunnel from site to site. To image the system, atoms are first pinned by ramping up the lattice depth to a value preventing any tunneling according to a simple and well-defined adiabaticity criterion, and subsequently exposed to fluorescence light allowing for the detection of each atom. Here, in contrast, we are interested in pinning the atoms of many-body systems that initially evolve in continuous space, whose projection dynamics is far more complex due to the absence of an initial energy gap and has not been studied to date. A first crucial challenge is therefore to ensure that the pinning of the many-body wave function preserves the collective information prior to pinning.

A second difficulty stems from light-assisted collisions that occur during imaging when two atoms occupy the same lattice site, such that quantum gas microscopy only gives access to the parity of the occupation number. In the study of Hubbard systems, the occupation is typically of one or two atoms per lattice site such that this parity projection can be mitigated [1,2]. In contrast, the high densities typically used in bulk systems correspond to having tens to hundreds of atoms per lattice site, such that parity projection would be crippling for most quantitative measurements. This can be circumvented by working with extremely dilute clouds, with about 2 orders of magnitude lower densities. The associated challenge is to prepare samples at accordingly lower temperatures in order to reach the deep quantum degenerate regime. In practice, this requires temperatures in the range of 1–20 nK, which are below or at the lowest end of the temperatures typically reached in bulk quantum gases.

In this work, we tackle these two challenges and perform quantum gas microscopy in the continuum for the first time, which we describe in the following.

Single-atom imaging of ultradilute Fermi gases—Our experiment starts with a single-component noninteracting Fermi gas of ^{6}Li atoms confined in a "light sheet," a highly oblate optical dipole potential providing strong confinement in the vertical z direction [42,43]. In the xy plane, the light sheet provides a shallow Gaussian-like trap, which can be approximated by a harmonic potential near the trap center. The corresponding trapping frequencies are $\omega_x/2\pi \approx 30$ Hz, $\omega_y/2\pi \approx 80$ Hz, and $\omega_z/2\pi \approx 1.1$ kHz. In-plane density variations near the trap center are nonetheless small enough to extract homogeneous quantities, as is typically done in the framework of the local density approximation [44]. Having prepared the system with a given atom number ranging from $N = 45(7)$ to 325(21), we suddenly pin the atoms by ramping on a deep optical lattice in the xy plane and apply Raman sideband laser cooling, which reduces the motional energy of each atom in its lattice well and simultaneously drives their fluorescence. The scattered photons are collected through a high-resolution objective and projected onto a CCD camera [43].

The pinning phase, where atoms initially evolving in the continuum are projected onto the wells of the lattice, is crucial in our experiment. According to our previous work on single-atom wave packets [43], reliable pinning requires the lattice ramp-on time τ to satisfy the inequality $\omega^{-1} \ll \tau \lesssim a_L/v$, where ω is the lattice well frequency at the end of the ramp, a_L is the lattice spacing, and v is the characteristic velocity of the system. While there is no demonstration that this criterion is sufficient at the many-body level, we consider it as a minimal requirement. For

our Fermi gases, the relevant scale is set by the Fermi velocity v_F, spanning from 7 to 14 mm/s. Applying our criterion, we set the lattice ramp time to $\tau = 10$ μs (see [43]).

In Fig. 1(a), we show a typical experimental image of a noninteracting Fermi gas obtained with our quantum gas microscope. The cloud shown here contains $N = 331$ atoms and is one of our densest clouds, with an interparticle distance on the order of 5 times the lattice spacing. In this regime of diluteness, density correlation functions are readily accessible as depicted in Figs. 1(b) and 1(c). Since we are interested in density correlations of the homogeneous Fermi gas, we perform the analysis on a central region of the cloud where the local density $n(\mathbf{r})$ is constant within 7% and the local average Fermi wave vector $k_F(\mathbf{r}) = \sqrt{4\pi n(\mathbf{r})}$ is constant within 3.5% (see [41]).

In situ correlation measurements—While our images allow us to access density correlation functions up to the highest order set by the particle number, we focus here on extracting the two- and three-point density correlations. Their reduced forms respectively read

$$g_2(\mathbf{r}_1, \mathbf{r}_2) = \frac{\langle \psi^\dagger(\mathbf{r}_2)\psi^\dagger(\mathbf{r}_1)\psi(\mathbf{r}_1)\psi(\mathbf{r}_2)\rangle}{n^2} \tag{1}$$

and

$$g_3(\mathbf{r}_1, \mathbf{r}_2, \mathbf{r}_3) = \frac{\langle \psi^\dagger(\mathbf{r}_3)\psi^\dagger(\mathbf{r}_2)\psi^\dagger(\mathbf{r}_1)\psi(\mathbf{r}_1)\psi(\mathbf{r}_2)\psi(\mathbf{r}_3)\rangle}{n^3}, \tag{2}$$

with $\psi^\dagger(\mathbf{r}_i)$ and $\psi(\mathbf{r}_i)$ the fermionic field operators, $\mathbf{r}_i$ the position of the ith atom, and n the local average density. In an isotropic homogeneous system at a given temperature, g_2 only depends on $r = |\mathbf{r}_1 - \mathbf{r}_2|$ such that it can be expressed as a one-dimensional function, and g_3 only depends on the absolute distance $r_{12} = |\mathbf{r}_1 - \mathbf{r}_2|$ between two fermions labeled as 1 and 2, and the position of the third atom $\mathbf{r}_3$.

We start our analysis with Fermi gases that were prepared with the lowest atom numbers $N = 45(7)$. Near the center of the cloud, the average density is $n = 0.04$ μm^{-2}, the average interparticle spacing $d = 1/\sqrt{n} = 5.1$ μm, corresponding to an inverse Fermi wave vector $k_F^{-1} = 1.45$ μm, and a Fermi temperature $T_F = 19.3(1)$ nK, defined as $T_F = E_F/k_B = \hbar^2 k_F^2/(2mk_B)$, with E_F the Fermi energy, $\hbar$ the reduced Planck constant, m the particle mass, and k_B the Boltzmann constant.

In Fig. 1(d), we show the correlation function $g_2(k_F r)$ extracted from the analysis of 2500 images, along with a fit to the theoretical prediction at finite temperature (see [41]). This measurement alone contains several key pieces of information and demonstrates that the two aforementioned challenges have been overcome. Firstly, we observe a clear Fermi hole, which directly reveals that our clouds are degenerate while being in the regime of diluteness required to eliminate double occupancies to a high degree. More quantitatively, we obtain $T = 9.2(7)$ nK with an excellent fit to the experimental data, corresponding to $T/T_F = 0.47(4)$, using the absolute temperature T as the sole fitting parameter, since g_2 only depends on $k_F r$ and T/T_F, with k_F and T_F directly accessible via the measured density. Finally, the observation of a 100%-contrast Fermi hole matching the theoretical prediction indicates reliable pinning of the many-body wave function. If a fraction of atoms were recaptured at a random distance from their initial location upon pinning, the contrast would be reduced by an amount on the order of that fraction. While fermionic antibunching was observed in previous correlation measurements in momentum or time domain [45–47] and in lattice systems [48,49], the shape of the Fermi hole was never measured, to the best of our knowledge.

From the same set of images, we extract the three-point reduced density correlation function $g_3(k_F r_{12}, k_F \mathbf{r}_3)$, by selecting a pair of atoms and evaluating the probability to find a third atom at a given relative coordinate in the xy plane. Applying this procedure to all possible pairs within the central region of the cloud, we obtain density plots as shown in Fig. 2(a). To visually represent g_3, we set the origin of space between two fermions labeled 1 and 2, such that $\mathbf{r}_2 = -\mathbf{r}_1 = (r_{12}/2)\mathbf{e_x}$ and $\mathbf{r}_3 = x_3\mathbf{e_x} + y_3\mathbf{e_y}$. We show a set of g_3 functions in Fig. 2(b) for different values of the distance r_{12} that are all extracted from the same dataset, and which we represent both as density plots and as cuts taken at $y_3 = 0$. In the density plot, the position of the two fixed atoms is evident from the Fermi hole surrounding them. As the distance r_{12} is reduced from several times to a fraction of k_F^{-1}, we not only see the Fermi holes progressively merge but also the probability to find a third neighboring atom drastically drop. This observation provides a striking visualization of the Pauli exclusion principle: in an ideal Fermi gas, particles tend to maximize space occupation and the probability of finding two atoms or more within an area of radius $\lesssim k_F^{-1}$ is extremely small.

To test whether the two-point and three-point density correlation functions are mutually consistent and to what extent, we compare the cuts shown in Fig. 2(b) to the theoretical prediction at the temperature $T = 9.2(7)$ nK, which is the temperature obtained from fitting g_2, and find excellent agreement throughout the entire range of r_{12} values. Upon fitting the g_3 measurements to the theoretical prediction, leaving the absolute temperature as a free parameter, we find $T = 8.7(3)$ nK.

The ideal Fermi gas Hamiltonian being quadratic in creation and annihilation operators, Wick's theorem predicts that any correlation function can be expressed in terms of the coherence function $g_1(r) = \langle \psi^\dagger(0)\psi(r)\rangle/n$. Specifically, $g_2(r) = 1 - g_1(r)^2$ and $g_3(\mathbf{r}_1, \mathbf{r}_2, \mathbf{r}_3) = 1 - g_1(r_{12})^2 - g_1(r_{23})^2 - g_1(r_{31})^2 + 2g_1(r_{12})g_1(r_{23})g_1(r_{31})$,

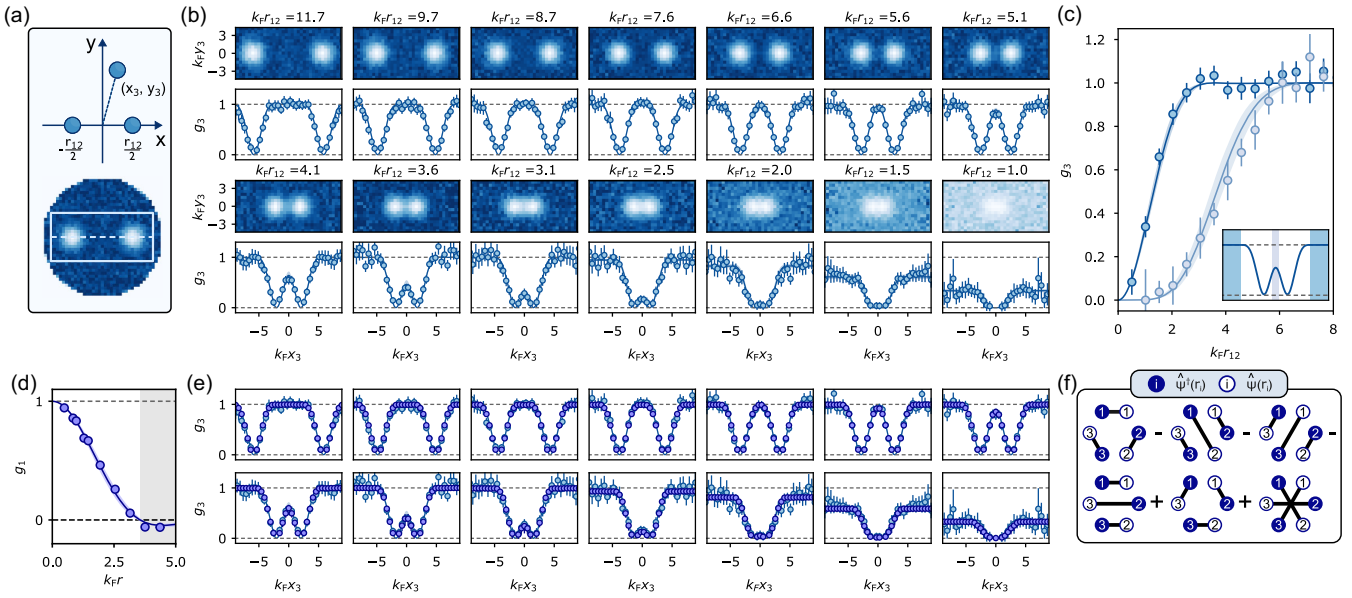

FIG. 2. Three-body correlation functions and Wick analysis. (a) Schematic showing the coordinate system definitions (top) and the region of g_3 plotted in the panels of (b) (bottom). (b) Density plots and central cuts of the g_3 correlation function for a noninteracting Fermi gas. Each panel consists of a 2D density plot of g_3 and a central cut ($y_3 = 0$, data points) similar to Fig. 1(e) at specific values of $k_F r_{12}$, indicated above each panel. (c) Average g_3 values as a function of $k_F r_{12}$ for two limiting cases, as illustrated by the inset. The dark blue data points show $\lim_{r_3 \to \infty} g_3(r_{12}, x_3, y_3)$. The light blue data points are taken from the center of each trace in (b), where $x_3 = y_3 \approx 0$. Solid lines in (b) and (c) show theory at the temperature obtained from the g_2 measurement, with shaded areas indicating uncertainties [41]. (d) Coherence function $g_1(r)$ extracted from the g_2 function through Wick's theorem. (e) Comparison between the directly extracted g_3 correlation function from (b) (blue data points) and the g_3 function obtained through application of Wick's theorem on the extracted g_1 from (d) (purple data points). (f) Visual representation of Wick's theorem applied to the g_3 correlation function. Blue (white) circles represent creation (annihilation) operators. Black lines represent the different contractions that allow g_3 to be expressed in terms of g_1 correlation functions.

where $r_{ij} = |\mathbf{r}_j - \mathbf{r}_i|$. Using these relations, we first extract the coherence function g_1 using the measured g_2 function (see [41]), which we show in Fig. 2(d), and in turn use g_1 to obtain g_3 for the various values of r_{12}. The resulting traces for $g_3(k_F r_{12}, x_3, y_3 = 0)$ are plotted in Fig. 2(e), showing a remarkable agreement with the measured correlation functions. This analysis, which does not rely on any fitting, not only shows that the measured g_2 and g_3 functions are mutually consistent to a high degree, but also represents a verification of Wick's theorem for these correlations in our samples.

Correlations in a quasi-2D Fermi gas—In the vertical direction the atomic motion is quantized, with a quantum of vibration corresponding to a temperature scale $T_z \equiv \hbar\omega_z/k_B = 54(4)$ nK. For the preparation discussed above, we ensured a minimal occupation of the excited z-level states by keeping T and T_F sufficiently smaller than T_z. We now deliberately prepare clouds for which higher z levels are occupied, by increasing T_F to values on the order of T_z, while keeping T low relative to both of these scales. For simplicity, we restrict ourselves to preparing samples where only the first excited z level is significantly occupied and the population in higher z levels is kept well below 1%. The total 2D correlation function can be obtained by summing over the z levels, and reads (see [41])

$$g_2^{\mathrm{tot}}(r) = 2p_0p_1 + p_0^2 g_2^{\{0\}}(r) + p_1^2 g_2^{\{1\}}(r), \qquad (3)$$

where p_ν is the fraction of atoms in the z level ν, and $g_2^{\{\nu\}}(r)$ the two-point reduced density correlation within this level. From Eq. (3) it follows that a nonzero population in $\nu = 1$ yields a nonzero value of the g_2 function at short distance, tending to $g_2^{\mathrm{tot}}(0) = 2p_0p_1$ for zero distance. The Fermi-hole contrast hence provides an excellent probe of the population on the first excited level. The result Eq. (3) can be generalized to an arbitrary number of populated excited states (see [41]), and represents a key new possibility for the exploration of low-dimensional quantum gases, where the determination of transverse state populations is typically nontrivial [50–54].

In Fig. 3(b) (top row), we show the total g_2 function obtained for samples with increasing Fermi energy. The data are fitted to Eq. (3) using T as the only free parameter (see [41]), showing excellent agreement and clearly demonstrating the reduction of the Fermi hole depth with increasing values of T_F. With the knowledge of T, we obtain not only the populations p_ν, but also both $g_2^{\{0\}}(r)$ and $g_2^{\{1\}}(r)$. The function $g_2^{\{0\}}(r)$ is shown in the bottom row of Fig. 3(b) providing a measure of the temperature dependence of the Fermi hole. The lower panels in Fig. 3

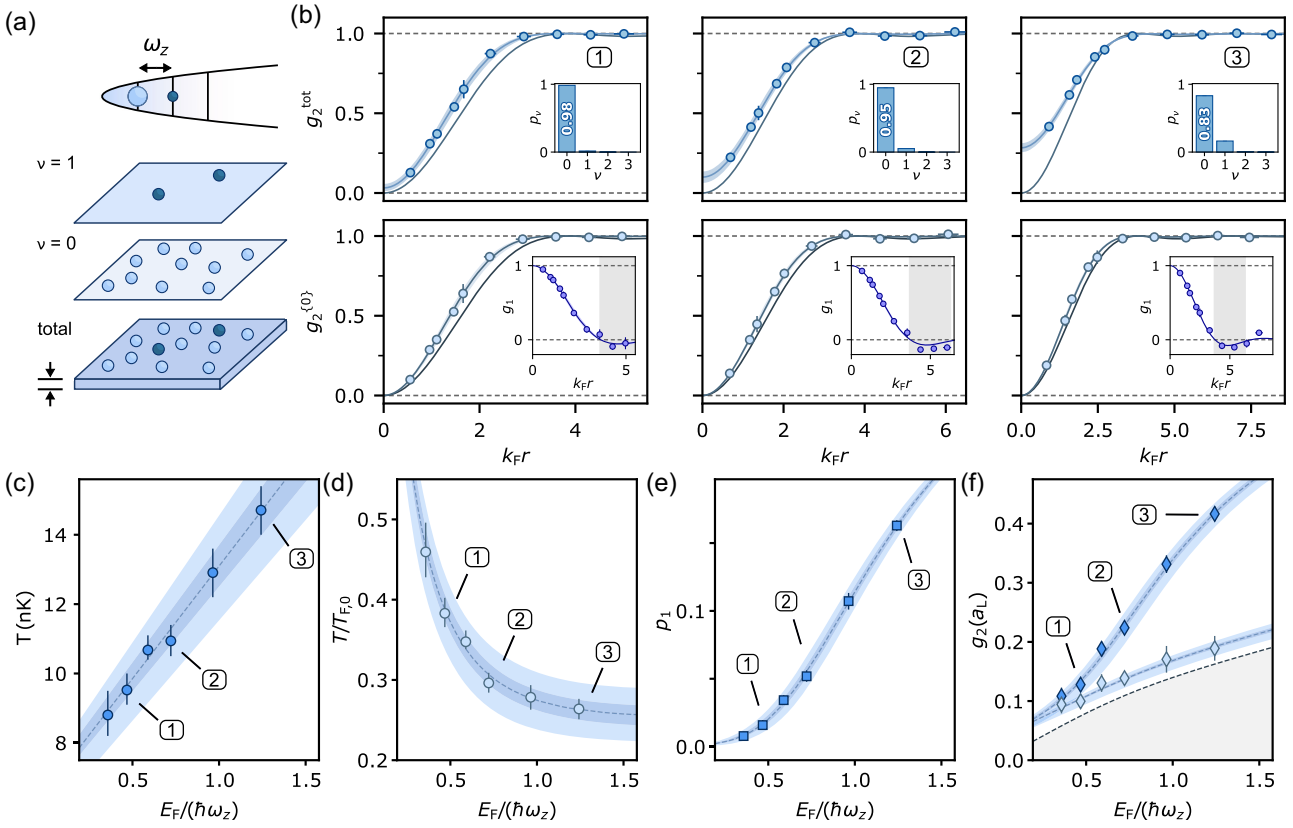

FIG. 3. Full characterization of a quasi-2D noninteracting Fermi gas. (a) Schematic representation of the two motional state populations in the vertical harmonic trap potential. Atoms in the $\nu = 0$ and 1 states are represented by the light and dark blue particles, respectively. (b) Top row: experimental g_2-correlation functions for $N = 71$, 142, and 325 atoms (data points)—labeled 1–3, respectively—with theoretical fits using T as the sole fitting parameter (blue curves). The shaded regions represent fitting uncertainties. Gray curves show the g_2 of a purely two-dimensional gas at $T = 0$. Error bars represent the standard error of the mean [41]. Insets show the distribution of the vertical level population obtained from the fit. Bottom row: $\nu = 0$ contribution to the g_2-correlation function for the respective top panels with insets showing the g_1-coherence function obtained from a Wick decomposition. (c)–(e) Temperatures (T), reduced temperatures of the $\nu = 0$ layer [$T/T_{F,0} = T/(T_F p_0)$], and p_1 values for systems prepared at different Fermi energies (E_F). The coldest point corresponds to the data presented in Figs. 1 and 2, reanalyzed with Eq. (3). Dashed lines are model-based guides to the eye, and dark (light) blue shaded areas indicate statistical (systematic) uncertainties; see [41]. (f) Value of g_2^{tot} (dark blue) and $g_2^{\{0\}}$ (light blue) at a distance of one lattice site (a_L). The gray dashed line shows the value of $g_2(a_L)$ in the pure-2D zero-temperature limit. Blue dashed lines and shaded areas serve as guides to the eye.

display all the relevant observables of the system and illustrate the power of our method as a diagnostic tool.

Conclusion and outlook—We have demonstrated quantum gas microscopy in the continuum. Key elements include the reliable pinning of the many-body wave function from continuous space, and performing parity-projection-free quantum gas microscopy by creating ultradilute degenerate bulk systems. We demonstrated the validity and the power of our imaging method via the measurement of two- and three-body density correlations of two-dimensional Fermi gases, which we found to be in excellent agreement with theoretical predictions and to satisfy Wick's theorem. These measurements represent the first *in situ* and atom-resolved spatial correlation measurements of a bulk gas, complementing previous work in momentum space [45–47,55] and work on temporal correlation functions in bosonic systems obtained with single-atom resolved measurements through electron impact ionization [56,57].

Our results extend the applicability of quantum gas microscopy to the realm of many-body physics in the continuum, offering a new set of possibilities for the exploration of strongly correlated quantum states. Our imaging method can be readily used to probe spin correlations in the 2D and 3D BEC-BCS crossover [58], and in particular in the paradigmatic unitary Fermi gas [24,25]. It provides a unique opportunity to facilitate the search for the elusive phases of matter such as the Fulde-Ferell-Larkin-Ovchinikov superfluid state [59,60], or quantum Hall states in rotating atomic gases beyond the few-particle regime

[15,61]. In combination with matter wave magnification techniques [14], our approach also makes the observation of crystaline order in 2D dipolar systems possible [62].

Note added—Recently, we became aware of related work on *in situ* studies of correlations in ultracold Fermi and Bose gases in the companion Letters [63,64]. Reference [65] reported microscopy of magnified few-fermion systems.

Acknowledgments—We thank Fabrice Gerbier and Martin Zwierlein for discussions, and Jean-Paul Nohra and Sebastian Will for a critical reading of the manuscript. We are grateful to Antoine Heidmann for his crucial support as head of Laboratoire Kastler Brossel. This work has been supported by Agence Nationale de la Recherche (Grant No. ANR-21-CE30-0021), CNRS (Tremplin@INP 2020), and Région Ile-de-France in the framework of DIM SIRTEQ and DIM QuanTiP.

[1] C. Gross and I. Bloch, Science **357**, 995 (2017).
[2] C. Gross and W. S. Bakr, Nat. Phys. **17**, 1316 (2021).
[3] A. M. Kaufman and K.-K. Ni, Nat. Phys. **17**, 1324 (2021).
[4] A. J. Daley, I. Bloch, C. Kokail, S. Flannigan, N. Pearson, M. Troyer, and P. Zoller, Nature (London) **607**, 667 (2022).
[5] W. S. Bakr, J. I. Gillen, A. Peng, S. Fölling, and M. Greiner, Nature (London) **462**, 74 (2009).
[6] J. F. Sherson, C. Weitenberg, M. Endres, M. Cheneau, I. Bloch, and S. Kuhr, Nature (London) **467**, 68 (2010).
[7] J. G. Danzl, M. J. Mark, E. Haller, M. Gustavsson, R. Hart, J. Aldegunde, J. M. Hutson, and H.-C. Nägerl, Nat. Phys. **6**, 265 (2010).
[8] B. Yan, S. A. Moses, B. Gadway, J. P. Covey, K. R. A. Hazzard, A. M. Rey, D. S. Jin, and J. Ye, Nature (London) **501**, 521 (2013).
[9] L. Christakis, J. S. Rosenberg, R. Raj, S. Chi, A. Morningstar, D. A. Huse, Z. Z. Yan, and W. S. Bakr, Nature (London) **614**, 64 (2023).
[10] S. L. Cornish, M. R. Tarbutt, and K. R. A. Hazzard, Nat. Phys. **20**, 730 (2024).
[11] A. N. Wenz, G. Zürn, S. Murmann, I. Brouzos, T. Lompe, and S. Jochim, Science **342**, 457 (2013).
[12] L. Bayha, M. Holten, R. Klemt, K. Subramanian, J. Bjerlin, S. M. Reimann, G. M. Bruun, P. M. Preiss, and S. Jochim, Nature (London) **587**, 583 (2020).
[13] M. Holten, L. Bayha, K. Subramanian, S. Brandstetter, C. Heintze, P. Lunt, P. M. Preiss, and S. Jochim, Nature (London) **606**, 287 (2022).
[14] S. Brandstetter, P. Lunt, C. Heintze, G. Giacalone, L. H. Heyen, M. Gałka, K. Subramanian, M. Holten, P. M. Preiss, S. Floerchinger, and S. Jochim, Nat. Phys. **21**, 52 (2025).
[15] P. Lunt, P. Hill, J. Reiter, P. M. Preiss, M. Gałka, and S. Jochim, Phys. Rev. Lett. **133**, 253401 (2024).
[16] H. Labuhn, D. Barredo, S. Ravets, S. de Léséleuc, T. Macrì, T. Lahaye, and A. Browaeys, Nature (London) **534**, 667 (2016).
[17] H. Bernien, S. Schwartz, A. Keesling, H. Levine, A. Omran, H. Pichler, S. Choi, A. S. Zibrov, M. Endres, M. Greiner, V. Vuletić, and M. D. Lukin, Nature (London) **551**, 579 (2017).
[18] W. B. Cairncross, J. T. Zhang, L. R. B. Picard, Y. Yu, K. Wang, and K.-K. Ni, Phys. Rev. Lett. **126**, 123402 (2021).
[19] A. Jenkins, J. W. Lis, A. Senoo, W. F. McGrew, and A. M. Kaufman, Phys. Rev. X **12**, 021027 (2022).
[20] C. M. Holland, Y. Lu, and L. W. Cheuk, Science **382**, 1143 (2023).
[21] M. W. Zwierlein, J. R. Abo-Shaeer, A. Schirotzek, C. H. Schunck, and W. Ketterle, Nature (London) **435**, 1047 (2005).
[22] M. W. Zwierlein, A. Schirotzek, C. H. Schunck, and W. Ketterle, Science **311**, 492 (2006).
[23] M. J. H. Ku, A. T. Sommer, L. W. Cheuk, and M. W. Zwierlein, Science **335**, 563 (2012).
[24] *The BCS-BEC Crossover and the Unitary Fermi Gas*, edited by W. Zwerger (Springer, Berlin, 2012), Vol. 836, 10.1007/978-3-642-21978-8.
[25] M. W. Zwierlein, in *Novel Superfluids*, edited by K. Bennemann and J. Ketterson (Oxford University Press, Oxford, 2013), Vol. II, pp. 269–422.
[26] Z. Hadzibabic, P. Krüger, M. Cheneau, B. Battelier, and J. Dalibard, Nature (London) **441**, 1118 (2006).
[27] J. V. José, *40 Years of Berezinskii-Kosterlitz-Thouless Theory* (World Scientific, Singapore, 2013), 10.1142/8572.
[28] R. Desbuquois, L. Chomaz, T. Yefsah, J. Léonard, J. Beugnon, C. Weitenberg, and J. Dalibard, Nat. Phys. **8**, 645 (2012).
[29] P. A. Murthy, I. Boettcher, L. Bayha, M. Holzmann, D. Kedar, M. Neidig, M. G. Ries, A. N. Wenz, G. Zürn, and S. Jochim, Phys. Rev. Lett. **115**, 010401 (2015).
[30] L. Sobirey, N. Luick, M. Bohlen, H. Biss, H. Moritz, and T. Lompe, Science **372**, 844 (2021).
[31] N. Navon, A. L. Gaunt, R. P. Smith, and Z. Hadzibabic, Science **347**, 167 (2015).
[32] J. Beugnon and N. Navon, J. Phys. B **50**, 022002 (2017).
[33] K. Lee, S. Kim, T. Kim, and Y. Shin, Nat. Phys. **20**, 1570 (2024).
[34] J.-R. Li, J. Lee, W. Huang, S. Burchesky, B. Shteynas, F. Ç. Top, A. O. Jamison, and W. Ketterle, Nature (London) **543**, 91 (2017).
[35] J. Léonard, A. Morales, P. Zupancic, T. Esslinger, and T. Donner, Nature (London) **543**, 87 (2017).
[36] F. Böttcher, J.-N. Schmidt, M. Wenzel, J. Hertkorn, M. Guo, T. Langen, and T. Pfau, Phys. Rev. X **9**, 011051 (2019).
[37] L. Chomaz, D. Petter, P. Ilzhöfer, G. Natale, A. Trautmann, C. Politi, G. Durastante, R. M. W. van Bijnen, A. Patscheider, M. Sohmen, M. J. Mark, and F. Ferlaino, Phys. Rev. X **9**, 021012 (2019).
[38] A. Recati and S. Stringari, Nat. Rev. Phys. **5**, 735 (2023).
[39] N. Bigagli, W. Yuan, S. Zhang, B. Bulatovic, T. Karman, I. Stevenson, and S. Will, Nature (London) **631**, 289 (2024).
[40] G. C. Wick, Phys. Rev. **80**, 268 (1950).
[41] See Supplemental Material at http://link.aps.org/supplemental/10.1103/PhysRevLett.134.183403 for additional details.
[42] S. Jin, K. Dai, J. Verstraten, M. Dixmerias, R. Alhyder, C. Salomon, B. Peaudecerf, T. de Jongh, and T. Yefsah, Phys. Rev. Res. **6**, 013158 (2024).
[43] J. Verstraten, K. Dai, M. Dixmerias, B. Peaudecerf, T. de Jongh, and T. Yefsah, Phys. Rev. Lett. **134**, 083403 (2025).

[44] Y. Castin, in *Lecture Notes of the 2006 Varenna Enrico Fermi School on Fermi Gases*, edited by M. Inguscio, W. Ketterle, and C. Salomon (IOS Press, Amsterdam, 2007), pp. 289–349, 10.3254/978-1-58603-846-5-289.
[45] T. Jeltes, J. M. McNamara, W. Hogervorst, W. Vassen, V. Krachmalnicoff, M. Schellekens, A. Perrin, H. Chang, D. Boiron, A. Aspect, and C. I. Westbrook, Nature (London) **445**, 402 (2007).
[46] P. M. Preiss, J. H. Becher, R. Klemt, V. Klinkhamer, A. Bergschneider, N. Defenu, and S. Jochim, Phys. Rev. Lett. **122**, 143602 (2019).
[47] K. F. Thomas, S. Li, A. H. Abbas, A. G. Truscott, and S. S. Hodgman, Phys. Rev. Res. **6**, L022003 (2024).
[48] L. W. Cheuk, M. A. Nichols, K. R. Lawrence, M. Okan, H. Zhang, E. Khatami, N. Trivedi, T. Paiva, M. Rigol, and M. W. Zwierlein, Science **353**, 1260 (2016).
[49] T. Hartke, B. Oreg, N. Jia, and M. Zwierlein, Phys. Rev. Lett. **125**, 113601 (2020).
[50] Z. Hadzibabic, P. Krüger, M. Cheneau, S. P. Rath, and J. Dalibard, New J. Phys. **10**, 045006 (2008).
[51] S. Tung, G. Lamporesi, D. Lobser, L. Xia, and E. A. Cornell, Phys. Rev. Lett. **105**, 230408 (2010).
[52] T. Yefsah, R. Desbuquois, L. Chomaz, K. J. Günter, and J. Dalibard, Phys. Rev. Lett. **107**, 130401 (2011).
[53] T. Yefsah, Thermodynamique du gaz de Bose à deux dimensions, Ph.D. thesis, Université Pierre et Marie Curie —Paris VI, 2011.
[54] C. De Daniloff, M. Tharrault, C. Enesa, C. Salomon, F. Chevy, T. Reimann, and J. Struck, Phys. Rev. Lett. **127**, 113602 (2021).
[55] R. Chang, Q. Bouton, H. Cayla, C. Qu, A. Aspect, C. I. Westbrook, and D. Clément, Phys. Rev. Lett. **117**, 235303 (2016).
[56] V. Guarrera, P. Würtz, A. Ewerbeck, A. Vogler, G. Barontini, and H. Ott, Phys. Rev. Lett. **107**, 160403 (2011).
[57] A. Vogler, R. Labouvie, F. Stubenrauch, G. Barontini, V. Guarrera, and H. Ott, Phys. Rev. A **88**, 031603(R) (2013).
[58] C. Daix *et al.* (to be published).
[59] P. Fulde and R. A. Ferrell, Phys. Rev. **135**, A550 (1964).
[60] A. I. Larkin and Y. N. Ovchinnikov, Sov. Phys. JETP **20**, 762 (1965).
[61] J. Léonard, S. Kim, J. Kwan, P. Segura, F. Grusdt, C. Repellin, N. Goldman, and M. Greiner, Nature (London) **619**, 495 (2023).
[62] H. P. Büchler, E. Demler, M. Lukin, A. Micheli, N. Prokof'ev, G. Pupillo, and P. Zoller, Phys. Rev. Lett. **98**, 060404 (2007).
[63] R. Yao, S. Chi, M. Wang, R. J. Fletcher, and M. Zwierlein, companion Letter, Phys. Rev. Lett. **134**, 183402 (2025).
[64] J. Xiang, E. Cruz-Colón, C. C. Chua, W. R. Milner, J. de Hond, J. F. Fricke, and W. Ketterle, companion Letter, Phys. Rev. Lett. **134**, 183401 (2025).
[65] S. Brandstetter, C. Heintze, K. Subramanian, P. Hill, P. M. Preiss, M. Gałka, and S. Jochim, arXiv:2409.18954.